ISSN 1028-334X, Doklady Earth Sciences, 2017, Vol. 473, Part 1, pp. 313–317. © Pleiades Publishing, Ltd., 2017.
Original Russian Text © S.V. Gladyshev, V.S. Gladyshev, A.V. Sokov, S.K. Gulev, L.A. Pautova, A.B. Demidov, 2017, published in Doklady Akademii Nauk, 2017, Vol. 473, No. 1, pp. 93–97.

OCEANOLOGY

Average Annual Structure and Transport of Waters Eastward of Greenland by the System of Western Boundary Currents

S. V. Gladyshev*, V. S. Gladyshev, A. V. Sokov,
Corresponding Member of the RAS S. K. Gulev, L. A. Pautova, and A. B. Demidov

Received March 29, 2016

Abstract—The results of calculating the values of average annual transport of waters eastward of Greenland in 2007–2015 by the system of western boundary currents are discussed. It is shown that the values of the average annual transport of waters estimated by different methods for measuring the velocity of currents and the different calculation methods differ by 20%. The role of friction in the bottom jets of the northwestern deep water, which were discovered for the first time during long-term observations, is discussed. The considerable contribution of the shelf water cascading across the continental slope to the formation of the structure and transport of the East Greenland Current is established. The significant influence of vertical mixing on the physicochemical properties of the bottom layer waters is shown. The biological arguments of the contribution made by the Irminger current and the subsurface waters to the formation of the northwestern deep water are presented.

DOI: 10.1134/S1028334X17030035

The system of western boundary currents (WBCs) is a key component of the lower segment in the North Atlantic meridional circulation that transports cold and relatively fresh waters to the south and the branched flow of warm and salt waters of the North Atlantic Current to the Arctic. The WBC system is the main source forming the North Atlantic Deep Water that has a global minimum of salinity in the Atlantic and Southern oceans. Monitoring of the WBC system is an effective method to observe the global changes in the World Ocean on climate time scales. This is exactly why the WBC is the most studied component of the North Atlantic subpolar gyre [1–8]. The long-term observations of the WBCs have shown insignificant interannual variations, but have not revealed any long-period trends in the volumes of water transport [9]. The calculations of this fundamental parameter of the WBCs according to the data measured by different groups of researchers demonstrate a difference of four times (4–16 Sv) in the values of transport for the bottom layer waters ($\sigma_\theta > 27.8$ kg/m^3) and a difference of almost three times (12–34 Sv) in the upper layer ($\sigma_\theta < 27.8$ kg/m^3) [8]. This difference is explained in part by the different methods of measuring the current velocity and the different methods of calculating this parameter.

Shirshov Institute of Oceanology, Russian Academy of Sciences, Moscow, 117218 Russia
**e-mail: sgladyshev@ocean.ru*

This work presents the results of calculating the values of the average annual transport of the WBC and its main structural components based on the results of direct measurements of the currents using the vessel-mounted ADCPs (OS38 and OS75 kHz in 2009–2015) and a pair of submersible ADCPs (Workhorse Sentinel and Monitor 300 kHz in 2007–2015) at the transatlantic section along 59.5° N that is recorded every summer, as well as using the daily data on the surface of the absolute geostrophic currents that are calculated from the satellite altimetry data with a space resolution of 1/4° (http://www.aviso. oceanobs.com). We also discussed new stable components of the WBC structure that were found in the bottom layer of the Irminger Sea.

The absolute geostrophic currents were calculated according to the procedures in [4, 8, 10] with subsequent interpolation of a grid with horizontal and vertical resolutions of 10 km and 10 m. The average annual currents were obtained by averaging the absolute geostrophic currents in the annual sections in each node of the grid. The averaging of nine sections makes it possible to minimize manifestations of synoptic variability and to reveal stable components of the gyre.

The calculations of the absolute geostrophic currents by the different methods provide a qualitatively similar scheme of the spatial WBC structure except for one important detail. The satellite altimetry does not enable us to distinguish between the coastal East Greenland Current (cEGC), the East Greenland Current (EGC), and the Irminger Current (IC) despite

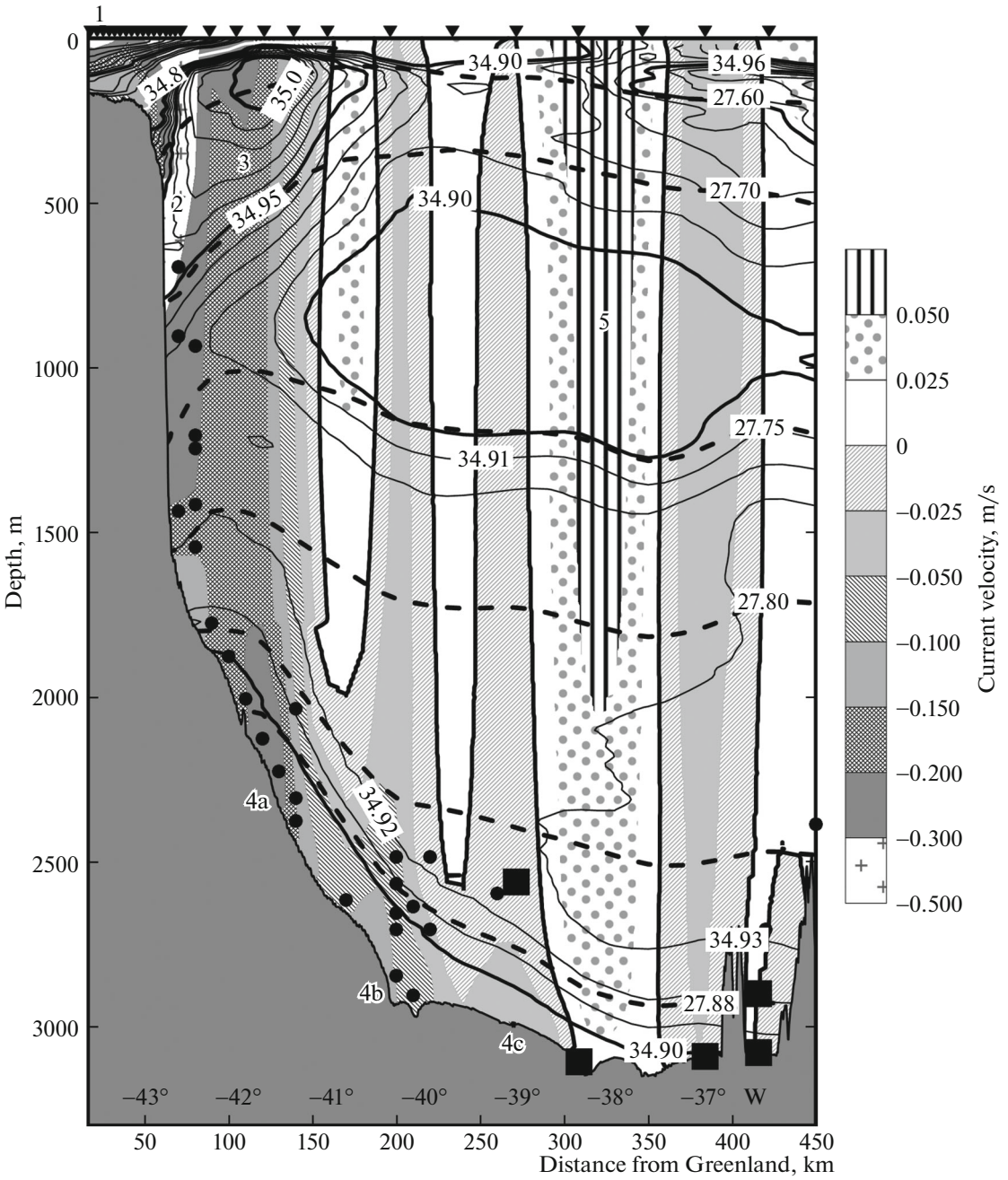

Fig. 1. Annual average kinematic structure (cross-hatched, m/s) and vertical distribution of salinity (solid thin lines, PSU) of the western boundary current system eastward of Greenland between 59.5°–60° in 2007–2015. The 34.8 PSU isoline of salinity is a white thickened line. The dashed thickened lines denote the distribution of potential density, kg/m^3. The dots represent the regions of unstable currents (the gradient number Ri < 0.25). The triangles on the upper axis depict the standard position of the hydrological stations. The black squares show the horizons of the biological samples that contained living cells of phytoplankton. The main structural WBC components are numbered with Arabic numerals: 1, the cEGC; 2, the EGC; 3, the IC; 4a, 4b, and 4c, bottom jets of the NWDW; and 5, the eastern branch of the Irminger gyre (IG). The bottom relief is shown in gray.

the improved horizontal resolution of the new CNES-CLS 13 version as compared to the CNES-CLS 09 version that served as the basis for recent studies [4, 8]. The absolute geostrophic currents that were calculated using the LADCP and the vertical distribution of salinity comprehensively describe the principal water masses and the structural WBC components (Fig. 1). We note that, using measurements with a horizontal resolution of 10 miles or less on the eastern slope of Greenland, we identified for the first time the jets of the EGC (2 in Fig. 1) and of the IC (3 in Fig. 1) even for the average annual section. The slope EGC around

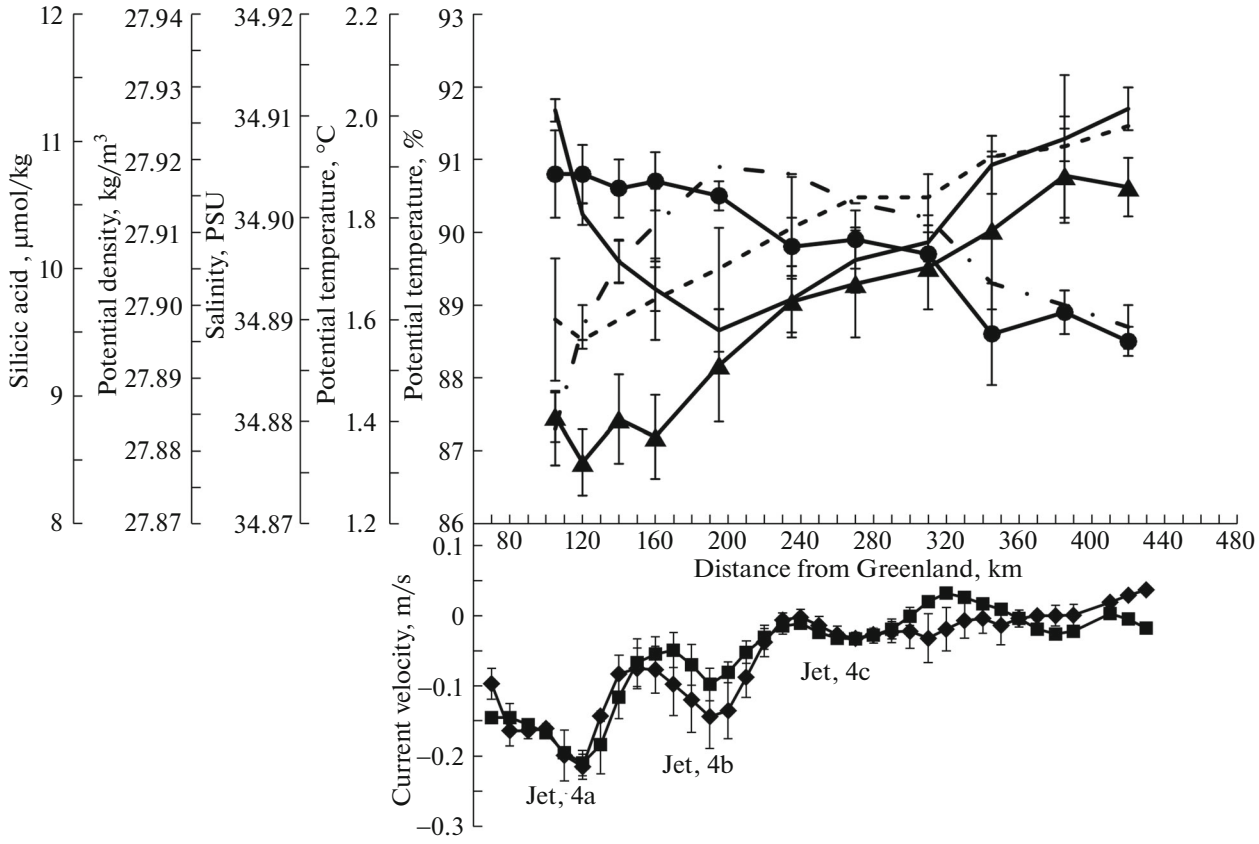

Fig. 2. Distribution of annual average potential temperatures (the solid line), salinity (the dashed line), potential density (the dot-and-dash line), oxygen saturation % (the line with dots), silicic acid (the line with triangles), and current velocity perpendicular to the section (the absolute geostrophic velocities according to the LADCP are shown by the line with squares, velocities measured by the LADCP are depicted by the line with the rhombi) in the NWDW layer of the Irminger Sea. The vertical lines depict errors in the calculations of characteristics.

60° N is composite and continues the current of the shelf margin in the upper segment of the slope (0–400 m). It is located somewhat seaward and coincides with the sharp thermohaline front. As it flows to the south, the upper segment of the flow becomes saltier due to mixing with the IC. This is confirmed by the position of the 34.8 PSU isohaline, which, according to [10], is a conventional boundary between the EGC and the IC. The bottom segment of the EGT (the intermediate layer of 400–1500 m between the isopycnals of 27.6–27.8 σ_θ) is formed by the waters of the jet that is called a "spill jet" in the international literature [3, 11]. This segment of the current is formed due to intense and regular (every 2–5 days) cascading of the shelf waters across the slope southward of the Denmark Strait [12, 13]. The surface-intensified IC is characterized by a subsurface salinity maximum >35.0 PSU and closely adjoins the EGC.

The dense waters cascading from the shelf regularly reach depths greater than 2000 m and form a stable slope deep jet of the WBC (4a, in Fig. 1) (the bottom layer around 60° N is characterized by the lowest salinity and the 34.92 PSU isochaline can be taken as its upper boundary). Fig. 2. This jet strongly differs from the deeper jets (4b, 4c in Fig. 1) in its physicochemical characteristics. It is warmer (the IC influence) and fresh (the influence of shelf waters) and is much more saturated with oxygen due to the recent contact with the surface waters. Along the entire slope, especially in the region of deep jets, the gradient Richardson number $\mathrm{Ri} = [N(x, z)/u_z(x, z)]^2$, where N is the Brunt–Väisäla frequency and $u_z < 0.25$ is the vertical gradient of the LADCP velocity. This points to intense mixing in these regions. The comparison between the vertical profiles of the absolute geostrophic and measured current velocity that is perpendicular to the section indicates a significant deviation of the latter from the geostrophic values. A great influence on the structure of the bottom-intensified jets is exerted by friction. In the Blasius problem on flow past an infinite horizontal plate by the turbulent flow [14], the height of the bottom boundary layer H^* (a friction layer) can be estimated as $H^* = 0.015(\mu/\rho U)^{1/7}x^{6/7}$, where μ is the dynamic viscosity of the medium (in our case, it is considered equal to 10^{-3} Pa s), ρ is the distinctive density (~1027.9 kg m^{-3}), U is the distinctive velocity

Average values of water transport (Sv) by the WBC system in 2007–2015

WBC structures	Vertical layer	Abs. geo. LADCP	Abs. geo. SADCP	Abs. geo. altimetry	LADCP measurements	Avg.
cEGC (10–50 km)	All water column	1.3 ± 0.5	1.7 ± 0.8	0.7 ± 0.4**	1.3 ± 0.6	1.3 ± 0.6**
EGC (50–90 km)	Upper segment of the MTC, $\leq 27.6\sigma_\theta$	3.7 ± 0.4	4.3 ± 0.6	3.0 ± 0.4	3.9 ± 0.3	3.7 ± 0.4
	Lower segment of the MTC, $27.6–27.8\sigma_\theta$	9.5 ± 1.2	10.4 ± 1.7	8.3 ± 1.4	9.3 ± 1.4	9.4 ± 1.4
	Total transport by the EGC	13.2 ± 0.9	14.7 ± 1.3	11.3 ± 1.0	13.2 ± 1.0	13.1 ± 1.0
IC (90–160 km)	Upper segment of the MTC, $\leq 27.6\sigma_\theta$	1.2 ± 0.3	1.5 ± 0.4	1.0 ± 0.1	1.3 ± 0.3	1.3 ± 0.3
	Lower segment of the MTC, $27.6–27.8\sigma_\theta$	9.1 ± 2.7	8.6 ± 3.3	5.7 ± 1.4	9.8 ± 2.6	8.3 ± 2.6
	Lower segment of the MTC, >27.8, >34.92, NEDW	0.7 ± 0.4	0.6 ± 0.3	0.3 ± 0.1	0.8 ± 0.6	0.6 ± 0.4
	Total transport by the IC	11.0 ± 1.6	10.7 ± 1.9	7.0 ± 0.8	11.9 ± 1.5	10.2 ± 1.5
NWDW (70–430 km)	Lower segment of the MTC, >27.8, ≤34.92	9.3 ± 4.1	8.1 ± 6.1	7.7 ± 2.9	10.1 ± 4. 8	8.8 ± 4.6
	Jet 4a (80–160 km)	6.7 ± 1.5	6.8 ± 1.9	3.1 ± 0.7	4.2 ± 0.6	5.2 ± 1.3
	Jet 4b (160–240 km)	1.9 ± 0.9	1.8 ± 1.4	2.0 ± 0.5	3.8 ± 1.2	2.4 ± 1.1
	Jet 4c (240–330 km)	0.4 ± 0.5	0.1 ± 0.3	0.3 ± 0.3	0.6 ± 1.0	0.3 ± 0.6
Eastern periphery of the Irminger Gyre (270–350 km)	Upper segment of the MTC, $\leq 27.6\sigma_\theta$	0.6 ± 0.3	1.6 ± 0.9	0.6 ± 0.3	0.6 ± 0.4	0.9 ± 0.5
	Lower segment of the MTC, $27.6–27.8\sigma_\theta$	5.5 ± 1.1	10.8 ± 2.6	5.8 ± 0.9	6.1 ± 1.6	7.1 ± 2.4
	Lower segment of the MTC, >27.8, >34.92, NWDW	2.5 ± 1.8	4.6 ± 2.9	2.7 ± 1.4	2.3 ± 2.2	3.0 ± 2.1
	Total transport by the Irminger Gyre	8.6 ± 1.2	17.0 ± 2.3	9.1 ± 1.0	9.0 ± 1.6	10.9 ± 1.6
Total transport (0–270 km)	All water column	34.8 ± 5.9	35.2 ± 8.2	26.7 ± 3.4	36.5 ± 6.7	33.3 ± 6.3***

*The calculations are performed for 2009–2015. ** The estimation of average transport by the cEGC in the last column does not take into account the rate of current transport based on satellite altimetry. *** The estimation of total transport by the WBC does not take into account transport northwards by the eastern periphery of the Irminger Gyre. The MTC is the meridional thermohaline circulation; abs. geo. LADCP is the annual average absolute geostrophic currents with the barotropic component calculated from the LADCP data; abs. geo. SADCP is the annual average absolute geostrophic currents with the barotropic component calculated from the SADCP data; abs. geo. altimetry is the annual average absolute geostrophic currents with the barotropic component calculated from the satellite altimetry data; and LADCP measurements are averaged data measured by a pair of LADCPs.

(~0.2 m s^{-1}), and x is the length of the segment where the flow exists. Depending on the x-values (300–800 km), the boundary layer height is 120–300 m and corresponds to its height recorded at 100–200 m.

In the phytoplankton samples taken from the bottom layer of the Irminger Sea at the depths of 2560–3106 m, we found singular living cells of the warm-water centric diatom *Rhizosolenia hebetata* (Fig. 1). The result is biological confirmation of two important conclusions. First, the IC is the most likely source of warm-water cells, which confirms its important role in the formation of the northwestern deep water (NWDW) when it flows over the sill in the Denmark Strait. Secondly, the near-surface waters of the photic layer participate in the NWDW formation over the Denmark sill. It is stated in [15] that the diatom cells exist in a wet state with no exposure to light for about three months. Some cells contained "yellow" chromatophores in the bottom layer, which indicates chlorophyll degradation when they were found in the aphotic zone and reached the survival limit under such conditions. Taking into account the calculated velocities of the NWDW, this time is quite sufficient for

60° N and could be reached after the formation over the Denmark sill.

The table shows the estimates of the annual average transport by the WBC system and its separate elements according to the results of direct measurements using the LADCP and the absolute geostrophic currents calculated by different methods. The calculation errors were estimated by the standard deviation from the mean. The horizontal scales of the currents in the first and second columns of the table are determined for the absolute geostrophic values calculated from the LADCP measurements and may differ by 10–20 km for the currents calculated by other methods. When estimating the values of transport by the cEGC, the EGC, and the IC obtained using the satellite altimetry, we used the lateral dimensions from the table. Intense mixing shown in Fig. 1 makes the selected vertical boundaries of the layers and water masses sufficiently conventional. For example, it follows from the table that the transport of the North Atlantic deep water (NADW) by the IC is the smallest; in this case, the contribution of this water mass to the formation of the less dense NWDW on the continental slope of Greenland is not estimated (Fig. 1). The analysis of the results in the table allows us to make the following short conclusions.

(1) There is a 20% difference in the values of water transport estimated by the different calculation methods.

(2) The contribution of cascading ("spill jet") to the transport of the EGC at 60° N to 70% was 9.4 ± 1.4 Sv, which is almost two times greater than the average "spill jet" transport at 65° N [3]. Such an increase may relate to the existence of other cascading sources between 60°–65° N.

(3) The average values of transports are close to the average estimates obtained in [8] for the section of 59.5° N in 2002–2008.

ACKNOWLEDGMENTS

This work was supported by the Russian Science Foundation (project no. 14–17–00697), and the analysis of the water transport values by the WBC system in the Irminger Sea was conducted with support of the Russian Foundation for Basic Research (project no. 15–05–02250).

REFERENCES

1. S. Bacon and P. Saunders, J. Phys. Oceanogr. **40**, 815–829 (2010). doi 10.1175/2009JPO4091.1
2. M. Bersch, Deep-Sea Res. **42**, 1583–1607 (1995). doi 10.1016/0967-0637(95)00071-D
3. J. A. Brearley, R. S. Pickart, and H. Valdimarsson, Deep-Sea Res. **63**, 1–19 (2012). doi 10.1016/j.dsr.2012.01.001
4. C. Gourcuff, P. Lherminier, H. Mercier, and P. Y. Le Traon, J. Atmos. Oceanic Technol. **28**, 1324–1337 (2011). doi 10.1175/2011JTECH0818.1
5. N. P. Holliday, S. Bacon, J. Allen, and E. L. McDonagh, J. Phys. Oceanogr. **39**, 1854–1870 (2009). doi 10.1175/2009JP04160.1
6. P. Lherminier, H. Mercier, and C. Gourcuff, J. Geophys. Res. **112**, C07003 (2007). doi 10.1029/2006JC003716
7. P. Lherminier, H. Mercier, and T. Huck, Deep-Sea Res. **57**, 1374–1391 (2010). doi 10.1016/j.dsr.2010.07.009
8. A. Sarafanov, A. Falina, and H. Mercier, J. Geophys. Res. **117**, C01014 (2012). doi 10.1029/2011JC007572
9. R. Dickson, S. Dye, and S. Jonsson, , in *Arctic-Subarctic Ocean Fluxes* (Springer, New York, 2008), p. 443–474. doi doi 10.1007/978-1-4020-6774-7_20
10. D. A. Sutherland and R. S. Pickart, Prog. Oceanogr. **78**, 58–77 (2008). doi 10.1016/j.pocean.2007.09.006
11. R. Pickart, D. J. Torres, and P. S. Fratantoni, J. Phys. Oceanogr. **35**, 1037–1053 (2005).
12. A. Falina, A. Sarafanov, and H. Mercier, J. Phys. Oceanogr. **42**, 2254–2267 (2012). doi 10.1175/JPO-D-12-012.1
13. W.-J. von Appen, I. Koszalha, and R. S. Pickart, Deep-Sea Res. **92**, 75–84 (2014). doi 10.1016/j.dsr.2014.06.002
14. L. G. Loitsyanskii, *Fluid Mechanics* (Gostekhizdat, Moscow, 1950) [in Russian].
15. T. J. Smayda and B. Mitchell-Innes, Mar. Biol. (Heidelberg, Ger.) **25**, 195–202 (1974). doi 10.1007/BF00394965

Translated by L. Mukhortova